JOURNAL OF MATERIALS SCIENCE 29 (1994) 3363–3371

Acoustic emission study of phase relations in low-Y_2O_3 portion of ZrO_2–Y_2O_3 system

V. SRIKANTH, E. C. SUBBARAO*
Materials Research Laboratory, The Pennsylvania State University, University Park, PA 16802, USA

The (metastable) tetragonal phase in 3–4 mol% Y_2O_3–ZrO_2 alloys undergoes a transition to the monoclinic form in the 200–300 °C temperature range. Microcracking due to the volume change at this transition has been detected in these compositions by sharp acoustic emission during heating. The phase change was confirmed by X-ray diffraction, dilatometry and scanning electron microscopy. The monoclinic $\rightleftharpoons$ tetragonal transition in ZrO_2–1 mol% Y_2O_3 alloy at 850–750 °C and the same phase change in 2, 3, 4 and 6 mol% Y_2O_3 compositions at the eutectoid temperature of about 560 °C was also clearly signalled by the acoustic emission counts during heating and cooling. There was no significant acoustic emission activity on heating and cooling the 9 and 12 mol% Y_2O_3 compositions, which are cubic. The acoustic emission data thus confirm the phase relations in the 1–12 mol% Y_2O_3 region, established by conventional methods such as differential thermal analysis, dilatometry and X-ray diffraction.

1. Introduction

Since the discovery of high fracture toughness in zirconia alloys containing a metastable tetragonal phase by Garvie *et al.* [1], there has been intense study of the parameters governing this property. Toughened zirconia finds many applications, e.g. as extrusion dies. The presence of the metastable tetragonal phase which transforms to the monoclinic form is the key factor for the toughening process. Toughened zirconia alloys with small amounts of Y_2O_3 are among the prime candidates as toughened ceramics due to the relative ease of retaining the tetragonal phase at room temperature [2–4]. The amount of the tetragonal phase retained was found to depend on density [3], critical grain size [3, 4] (which in turn depends upon Y_2O_3 content), the temperature from which the sample is cooled [2] and the rate of cooling. For example, higher density, smaller than critical grain size, heating in the tetragonal phase field and rapid cooling rate favour the retention of the tetragonal phase. Both thermodynamic and kinetic factors were discussed in connection with transformation toughening [5]. The decrease in fracture toughness of partially stabilized zirconia annealed at > 1000 °C has been attributed to coarsening of tetragonal grains beyond the critical size [6–8]. On the other hand, annealing at low temperatures (200–300 °C) was also found to drastically decrease the strength and fracture toughness of zirconia–yttria alloys [9–26]. The amount of monoclinic phase was observed to increase rapidly when annealed in the 150–200 °C region and decrease sharply when annealed above 300–400 °C. Thus a maximum amount of the monoclinic phase is detected by annealing around 250 ± 50 °C. The exact annealing temperature for maximum monoclinic phase depends upon the initial sintering temperature [2, 10–18], the amount of Y_2O_3 [10–18, 21–24], the presence of moisture [19–24, 27, 28], time [10–23], the gaseous environment [29] and grain size [2, 10–18, 28]. The conversion of the tetragonal phase into the monoclinic form starts at the surface and proceeds to the interior [2, 10–18, 21–23, 29, 30]. Various additives [10–18, 25, 26, 29, 30], e.g. Al_2O_3 and CeO_2, are shown to prevent or inhibit this phase transformation, presumably due to the presence of second-phase particles at the grain boundaries providing a constraint. Alternately, surface modification methods have also been suggested [31, 32]. The phase composition (m, t, c) in all these studies was established by X-ray diffraction intensities [33, 34]. Since the monoclinic phase has a larger volume than the tetragonal phase, the t $\rightarrow$ m transformation causes microcracks, [9–18, 21–23, 26, 30] which are detected by scanning electron microscopy [3, 10–18].

Microcracking in ceramics due to phase changes (e.g. ferroelectric $PbTiO_3$ [35], superconducting $YBa_2Cu_3O_{7-x}$ [36]) or anisotropic axial thermal expansion (e.g. $Ca_{1-x}Sr_xP_6O_{24}$ [37], Al_2TiO_5 [38, 39]) can be easily detected by acoustic emission techniques. The t–m phase transformation in pure zirconia was studied by the acoustic emission method as a sintered sample and loose powder were cooled [40]. One of the objectives of the present work is to detect the microcracking accompanying the t $\rightarrow$ m transition during low-temperature annealing by the acoustic emission method as samples are heated in the 100–450 °C range.

* Permanent address: Tata Research Development and Design Centre, 1 Mangadas Road, Pune 411 050, India.

0022–2461

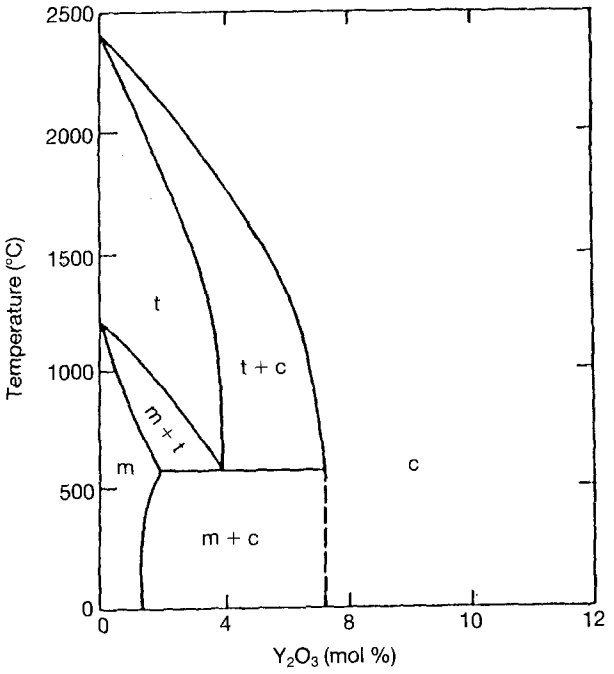

Figure 1 Low-yttria portion of the ZrO_2–Y_2O_3 phase diagram [4, 41, 42].

The phase diagram for the system ZrO_2–Y_2O_3 has been extensively investigated and an exhaustive review is presented by Yoshimura [41]. In the low-Y_2O_3 region, a number of investigations were carried out [42–45] and a generally agreed phase equilibrium diagram, proposed by Srivastava *et al.* [42], is shown in Fig. 1. At room temperature, one has monoclinic solid solution, $m_{ss} + c_{ss}$ and c_{ss} with increasing Y_2O_3 content. The t → m transition of ZrO_2 is lowered from 1170 °C to a eutectoid temperature at about 565 °C at a composition of about 3.5 to 4.0 mol% Y_2O_3. These phase relations are established by conventional methods employing differential thermal analysis, quenching, and X-ray diffraction. The fact that the tetragonal phase can be retained metastably at room temperature under certain circumstances has already been mentioned, but is not shown in Fig. 1. One of the objectives of the present work is to detect the phase transitions in ZrO_2–Y_2O_3 compositions with 1–12 mol% Y_2O_3 during heating (up to 1000 °C) and cooling by acoustic emission methods, and to substantiate the results obtained by dilatometry, X-ray diffraction and scanning electron microscopy.

Thus, acoustic emission methods are employed in the present work to detect (i) microcracking during low-temperature ageing due to the t–m transition in ZrO_2 alloys with 3–4 mol% Y_2O_3 and (ii) phase transitions during heating and cooling of 1–12 mol% Y_2O_3 compositions.

2. Experimental procedure

Zirconia and yttria with the characteristics given in Table I were mixed in appropriate amounts to make 1, 2, 3, 4, 6, 9 and 12 mol% Y_2O_3 compositions in a ball mill in polyethylene containers using ethyl alcohol as wetting agent and 1/2 in. (13 mm) diameter zirconia balls as grinding medium. The slurry was dried in an air oven at 80 °C for 24 h. The dried powders were calcined at 1500 °C. Later the calcined powder was pressed into pellets and pellets were sintered at 1700 °C for 4 h. The heating and cooling rates were 10 °C min^{-1}. X-ray diffraction study was carried out on powders using CuK_α radiation at 2°2θ min^{-1} scanning speed. The phase identification was based primarily on the $(\bar{1}\,1\,1)$ and $(1\,1\,1)$ reflections at $d = 0.318$ and 0.286 nm for the monoclinic, $(1\,1\,1)$ at $d = 0.296$ nm for the tetragonal and $(1\,1\,1)$ at $d = 0.295$ nm for the cubic phase.

For dilatometric measurements sintered pellets were cut into 25 mm × 5 mm × 5 mm. The samples and the two opposite faces of the specimen were polished flat and parallel. The heating rate was 10 °C min^{-1} and the cooling rate 2 °C min^{-1} in dilatometric runs (Harrop Industries model TD-716). Most of the measurements involved heating to 1000 °C and cooling to near room temperature. Some samples were cycled between room temperature and 1000 °C and room temperature and 450 °C to observe the transformation behaviour in detail.

For the acoustic emission study a sintered sample about 3 mm × 5 mm × 20 mm was attached with a high-temperature cement to a 30 cm long alumina rod which served as a waveguide. The other end of the alumina rod was joined to a transducer using a water-soluble ultrasonic couplant. The sample was placed inside a tube furnace and a Chromel–Alumel thermocouple positioned near the sample monitored the temperature. The furnace temperature was increased at 10 °C min^{-1} up to a temperature ranging from 450

TABLE I Characteristics of zirconia and yttria powders used

Zirconium oxide[a]	
L.O.I at 650 °C	0.48%
$ZrO_2 + HfO_2$[b]	99.7%
SiO_2	0.03%
FeO_3	< 0.015%
Na_2O	< 0.02%
CaO	< 0.02%
Cl	0.02%
SO_4	0.06%
Surface area (BET Method)	19 $m^2 g^{-1}$
Particle size (Sedigraph)	50% > 0.5 μm
Yttrium oxide	
Lu	< 50 p.p.m.
Gd	< 50 p.p.m.
Tm	< 50 p.p.m.
Yb	< 50 p.p.m.
Er	< 50 p.p.m.
Tb	< 50 p.p.m.
Dy	< 50 p.p.m.
Sm	< 50 p.p.m.
Ho	< 50 p.p.m.
Nd	< 100 p.p.m.
Si	< 100 p.p.m.
Fe	< 100 p.p.m.
Mg	< 100 p.p.m.
Ca	< 100 p.p.m.
Al	< 100 p.p.m.
Particle size	2–3 μm

[a] Typical average values from chemical analysis.
[b] ~ 2–3% HfO_2.

to 900 °C. The maximum temperature was maintained for 10 min, followed by cooling at 10 °C min^{-1} to 500 °C and at 2 °C min^{-1} to 100 °C. The transducer employed had a centre frequency of 500 kHz (in a range of 300 to 700 kHz). The electrical signal output from the transducer was amplified, filtered and processed through a train of instrumentation consisting of an amplifier, discriminator, totalizer and rate-meter modules to obtain data for total AE counts and the count rate (counts per 5 °C). The discriminator triggered a pulse whenever the amplifier output exceeded a certain adjustable threshold. The details of the system used here are described elsewhere [36, 37].

The fractured surfaces of as-sintered samples and after the dilatometric runs were observed on an ISI 60 scanning electron microscope.

3. Results and discussion

Two main aspects are presented here: (i) the metastable t → m phase transition at about 250 °C and (ii) phase relations in the ZrO_2–Y_2O_3 system from 1 to 12 mol% Y_2O_3. In both cases the discussion is based on data from X-ray diffraction, dilatometry and acoustic emission, supplemented in some cases by scanning electron micrographs. Of these, acoustic emission is a novel technique to be employed for the study of phase relations in the ZrO_2–Y_2O_3 system.

3.1. Metastable tetragonal → monoclinic phase transition

The X-ray diffraction patterns of sintered samples with 3, 4 and 6 mol% Y_2O_3 are shown in Fig. 2. The monoclinic phase decreases as the cubic phase content increases with increasing Y_2O_3 content. The relative amount of the metastable tetragonal phase is large in 3 and 4 mol% Y_2O_3 compositions and is essentially absent in the 6 mol% Y_2O_3 composition, in agreement with earlier reports. The thermal expansion behaviour of 3 and 4 mol% Y_2O_3 samples was determined by dilatometry up to 1000 °C in repeated cycles of heating and cooling. The data for ZrO_2–3 mol% Y_2O_3 are shown in Fig. 3 for two cycles of heating up to 1000 °C. During the first heating, there is an abrupt large expansion at about 250 °C, followed by very little expansion between 300 and 500 °C, beyond which there is a large contraction at about 550 °C and finally normal expansion beyond 600 °C. During cooling of this sample, the usual contraction down to about 400 °C is followed by a sudden large expansion, finally displaying a small contraction at temperatures below 200 °C. During the second cycle of heating there is a small expansion up to about 500 °C, then a sudden contraction, followed by the usual gradual expansion. Thus, during the second heating, the behaviour is similar to that in the first heating except for the absence of the sudden expansion at about 250 °C. The behaviour during cooling is nearly identical in the two cycles.

Similar data for a ZrO_2–4 mol% Y_2O_3 sample for three cycles of heating to 1000 °C and cooling are shown in Fig. 4. The behaviour of this sample is essentially the same as that of the 3 mol% Y_2O_3 sample and the data for the second and third cycles of heating and cooling reproduce well. These results are interpreted in terms of the presence of some amount of metastable tetragonal phase in these samples, which transforms to the (stable) monoclinic phase at about 250 °C accompanied by a large expansion. The contraction at about 550 °C on heating and expansion at about 400 °C on cooling represent the m → t → m transformations.

In order to gain further insight into this metastable t → m transformation at about 250 °C, the 4 mol% Y_2O_3 sample was studied up to 450 °C (with no

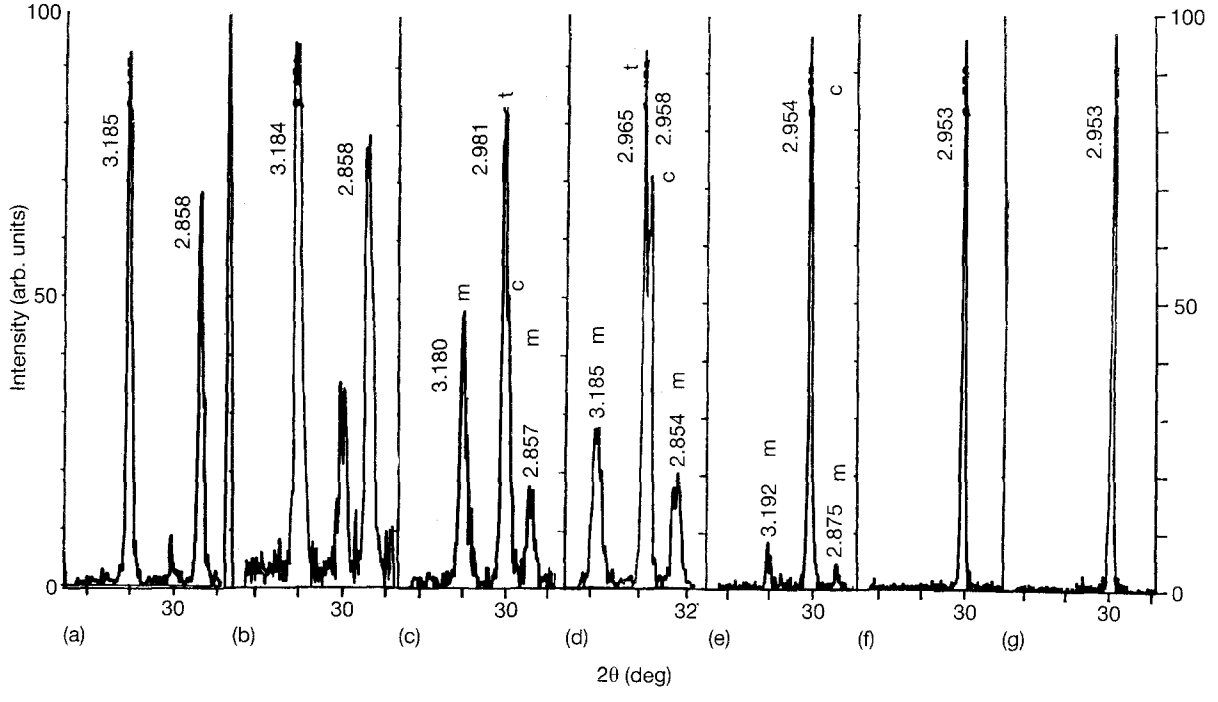

Figure 2 Portion of the X-ray diffraction patterns of (a) 1, (b) 2, (c) 3, (d) 4, (e) 6, (f) 9 and (g) 12 mol% Y_2O_3–ZrO_2 sintered compositions.

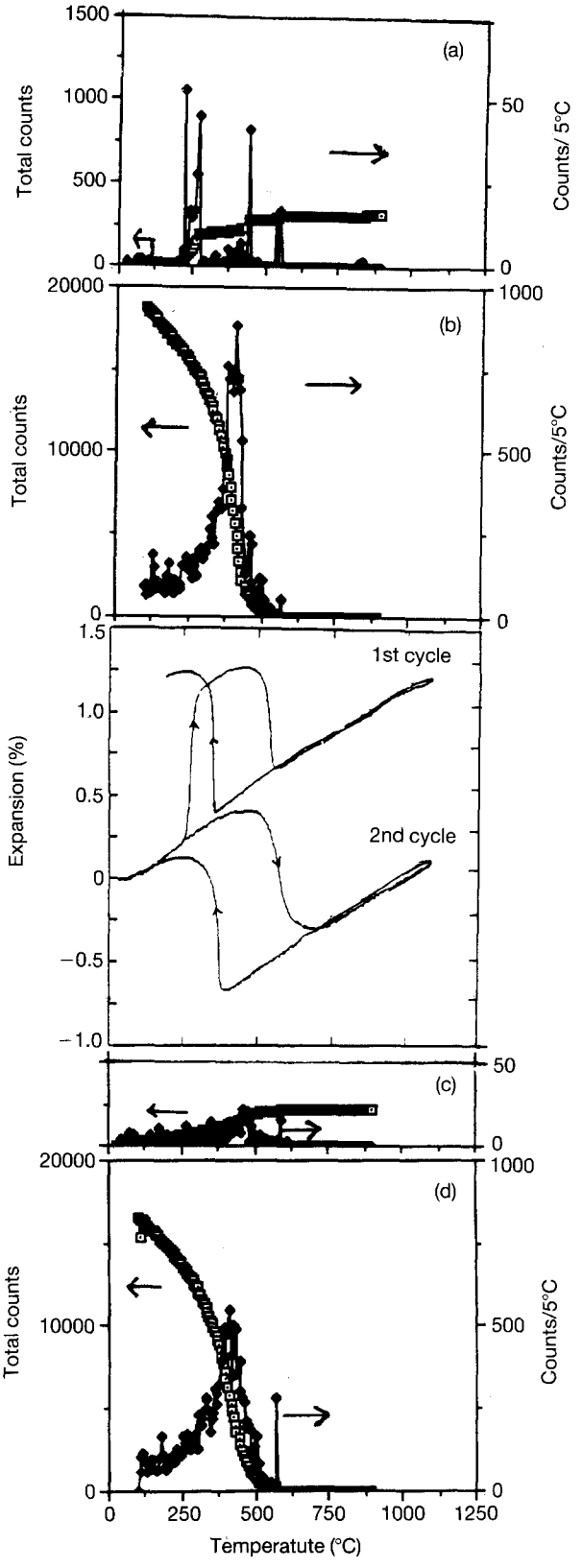

Figure 3 Thermal expansion behaviour of ZrO_2–3 mol% Y_2O_3 sample during two cycles of heating to 1000 °C and cooling (centre). The corresponding acoustic emission data (total counts and counts per 5 °C) in the first ((a) heating, (b) cooling) and second ((c) heating), (d) cooling) cycles are also shown: (⊡) total counts, (◆) counts per 5 °C.

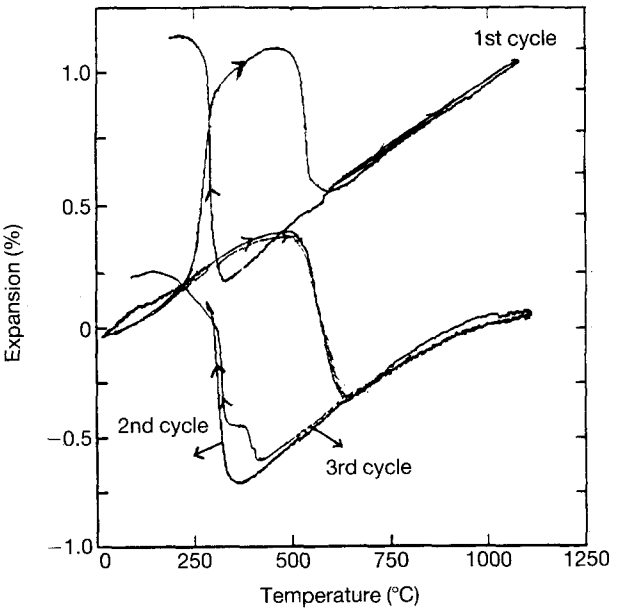

Figure 4 Thermal expansion behaviour of ZrO_2–4 mol% Y_2O_3 sample during three cycles of heating to 1000 °C, followed by cooling.

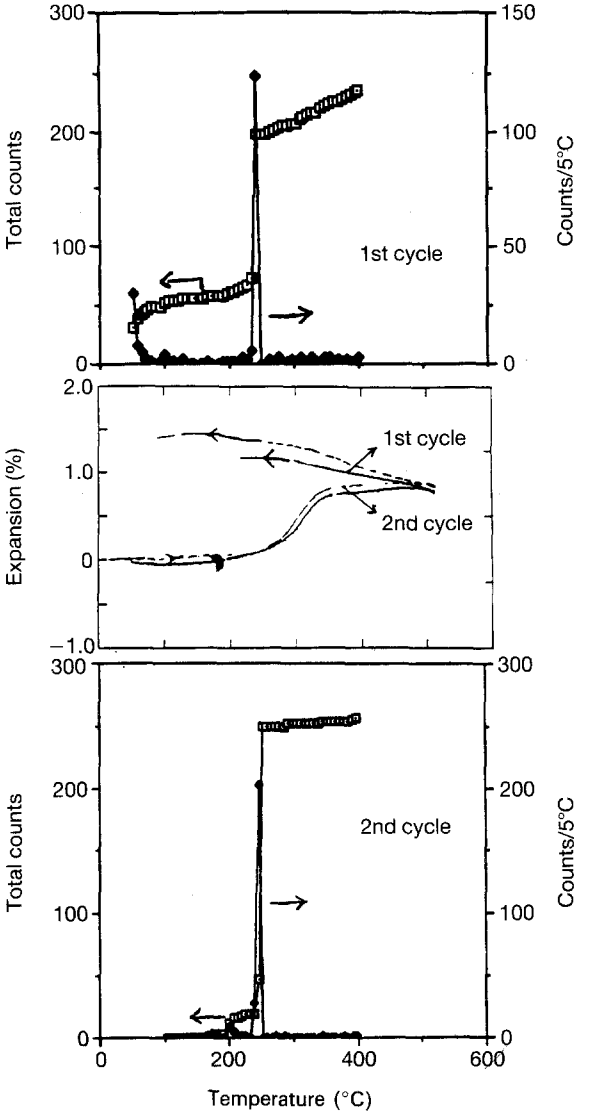

Figure 5 Thermal expansion behaviour of ZrO_2–4 mol% Y_2O_3 sample during two cycles of heating to 450 °C, followed by cooling. The corresponding acoustic emission data during heating in the two cycles are also shown: (⊡) total counts, (◆) counts per 5 °C.

holding time at the peak temperature) in two consecutive heating and cooling cycles (Fig. 5). The sample expands in the temperature range 250–350 °C, as noted before. On cooling from 450 °C, no dimensional anomalies are observed. Apparently, the

metastable tetragonal phase converts only partially into the monoclinic phase during the first heating up to 450 °C at the fast heating rate (10 °C min^{-1}) employed with no holding time at peak temperature. As a result, further transformation into the monoclinic phase takes place during the second heating cycle. It has been reported that annealing for about 20 h at 200 °C is necessary to obtain maximum conversion to the monoclinic phase in the 3 and 4 mol% Y_2O_3 samples. [10–18]. The present results are substantiated by the decrease of the X-ray diffraction intensity of the tetragonal reflection at 0.2965 nm of this sample after the first dilatometric experiment up to 450 °C, and its disappearance after the dilatometric experiment up to 1000 °C (Fig. 6), compared to that in the as-sintered condition. The X-ray diffraction intensity of the monoclinic phase increases relative to the tetragonal phase in the order: as-sintered, heated to 450 °C, and heated to 1000 °C. This clearly indicates that the monoclinic phase arises from conversion of the tetragonal phase and not from the cubic phase, in agreement with the results of Sato and Shimada [10].

These results are fully consistent with earlier reports [9–26] on the ageing or degradation of ZrO_2 samples with 3–4 mol% Y_2O_3 in the 200–400 °C temperature range due to conversion of the metastable tetragonal phase into the monoclinic form. The accompanying dimensional change is reported to cause microcracking [9–18, 21–23, 26, 30], which in turn results in a strength decrease. The presence of microcracks is plausible but is not easy to detect by microscopic techniques, though some indication of microcracks has been reported [3, 10–18]. In the present work, the acoustic emission method was employed for the detection of microcracks as these two samples were heated and cooled. The data (total counts and counts for 5 °C intervals) for the 3 mol% Y_2O_3 sample heated to and cooled from 1000 °C for two cycles are included in Fig. 3. The prominent acoustic emission activity in the 200–350 °C region detected during the first heating (Fig. 3a) is absent during the second heating (Fig. 3c), confirming that when the metastable t → m transformation is present extensive microcracking takes place due to the associated sudden dimensional change. The absence of similar activity in this temperature range during cooling (Fig. 3b and d) is consistent with this explanation.

Further confirmation of microcracking due to volume change associated with the metastable t → m phase change is obtained from acoustic emission data on heating the 3 mol% Y_2O_3 sample to 400 °C in two consecutive heating–cooling cycles (Fig. 7). Clearly there is a sudden, intense microcracking taking place around 250 °C during heating (Fig. 7a and c) which is absent during cooling (Fig. 7b and d). Further, the acoustic emission activity is less intense during the second heating to 400 °C (Fig. 7c) compared to that in the first cycle of heating (Fig. 7a), suggesting that much more of the metastable tetragonal phase present transforms to the monoclinic phase during the first

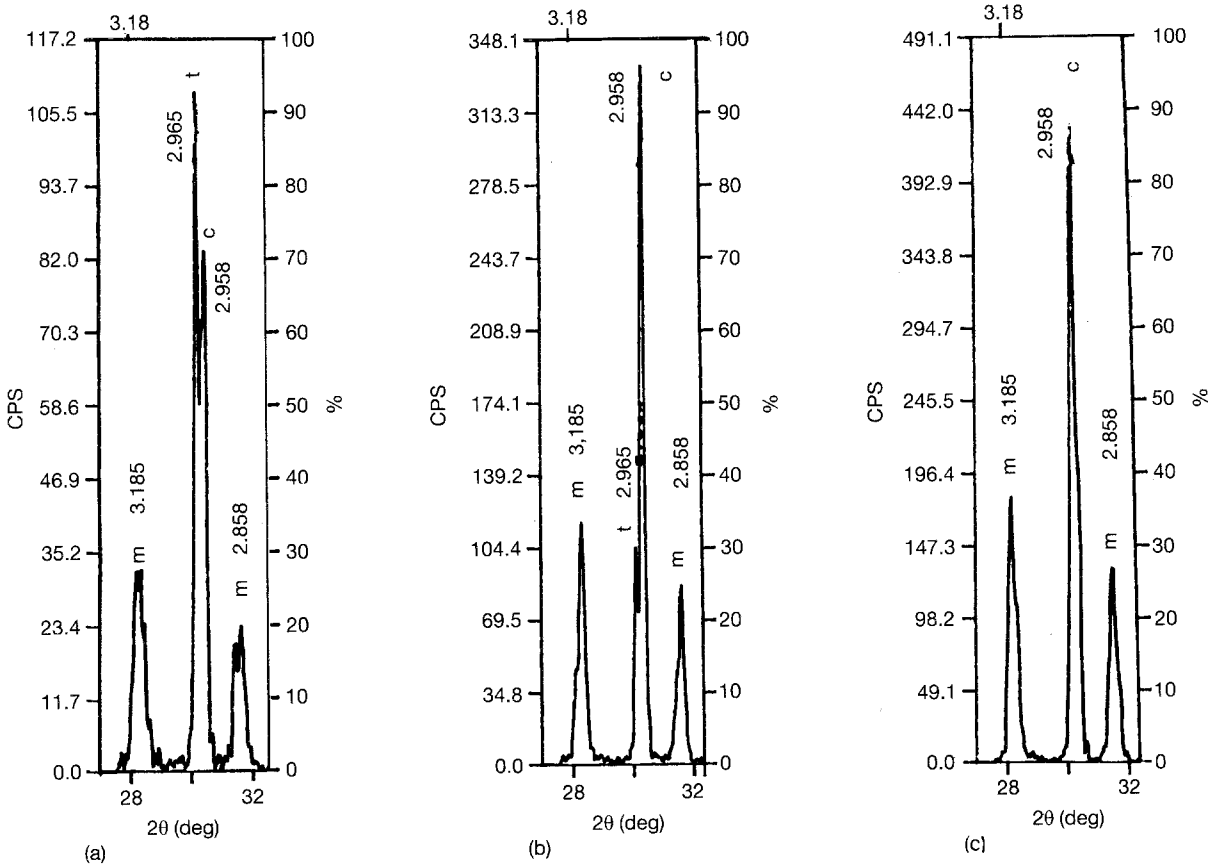

Figure 6 Portion of the X-ray diffraction patterns of ZrO_2–4 mol% Y_2O_3 sample (a) as sintered and after dilatometric runs up to (b) 450 °C and (c) 1000 °C.

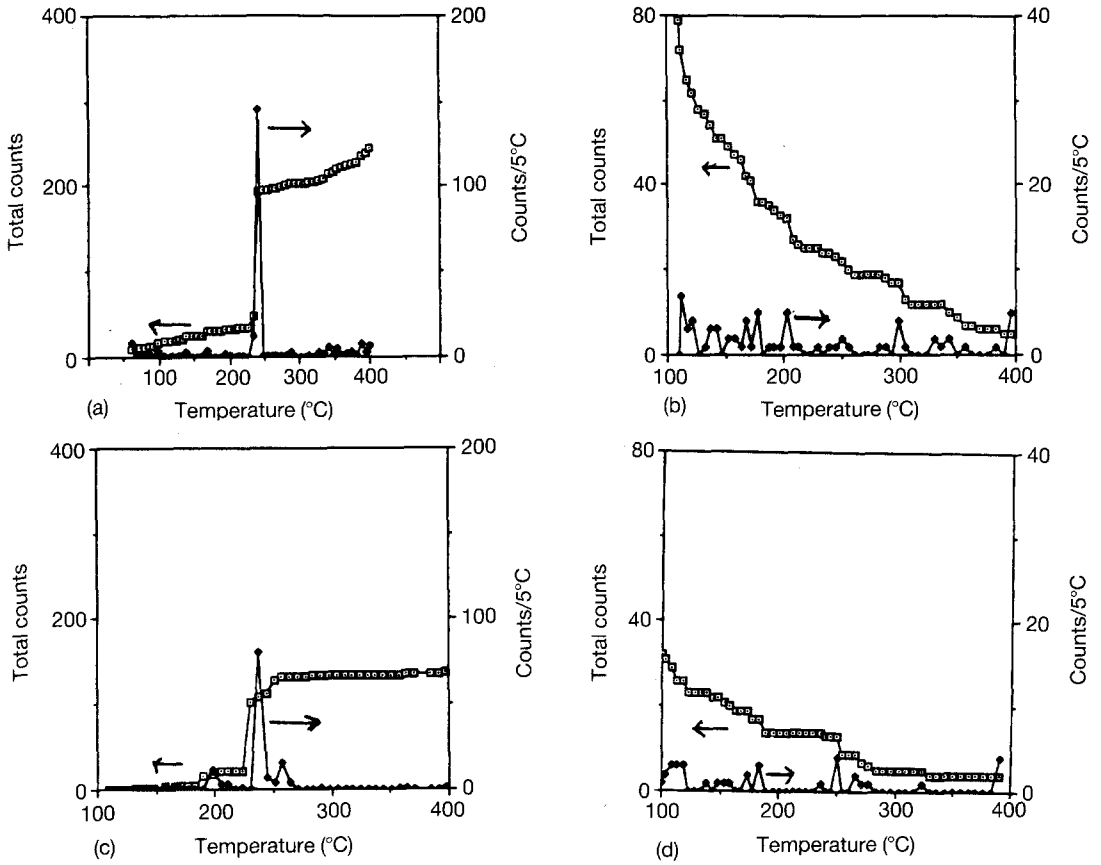

Figure 7 Acoustic emission data of ZrO_2–3 mol% Y_2O_3 sample (a, c) during heating to 400 °C and (b, d) cooling in two consecutive heating and cooling cycles: (⊡) total counts, (◆) counts per 5 °C.

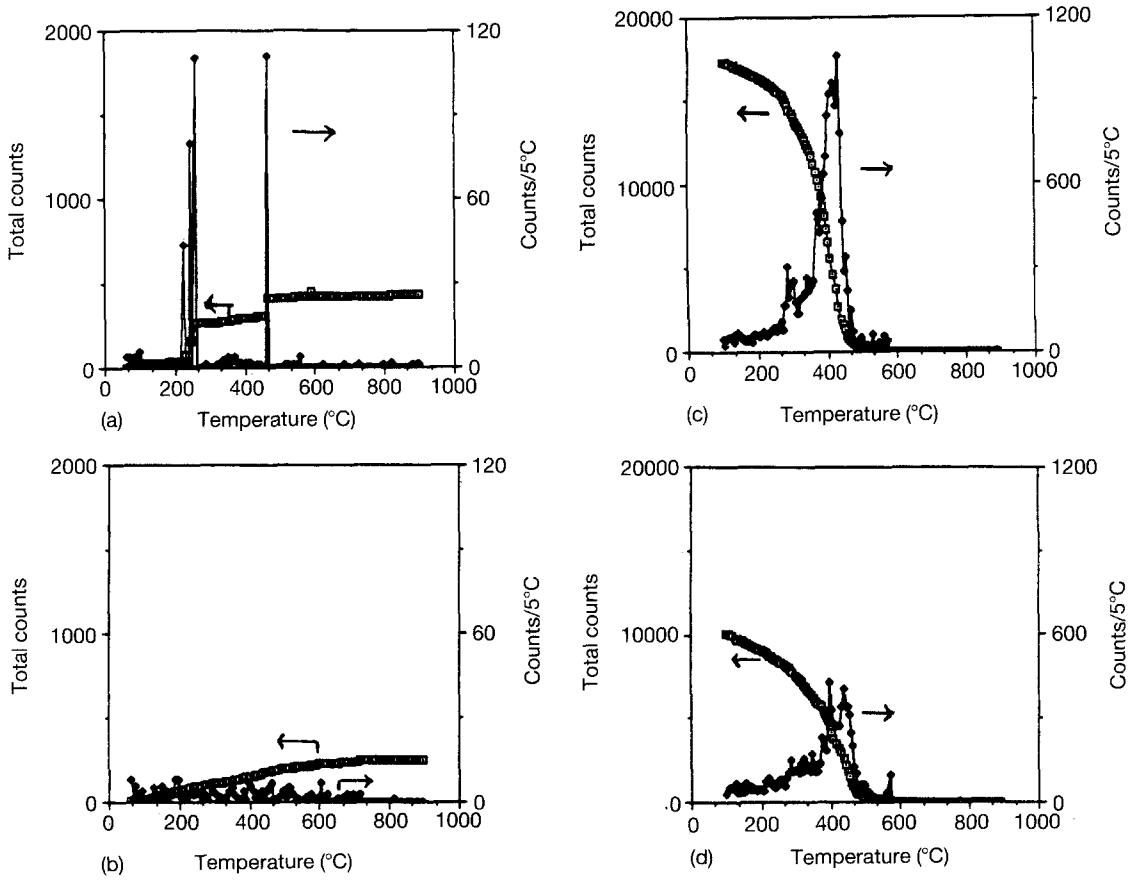

Figure 8 Acoustic emission data of ZrO_2–4 mol% Y_2O_3 sample (a, b) during heating to 900 °C and (c, d) cooling in two consecutive heating and cooling cycles: (⊡) total counts, (◆) counts per 5 °C. Refer to Fig. 4 for corresponding thermal expansion data.

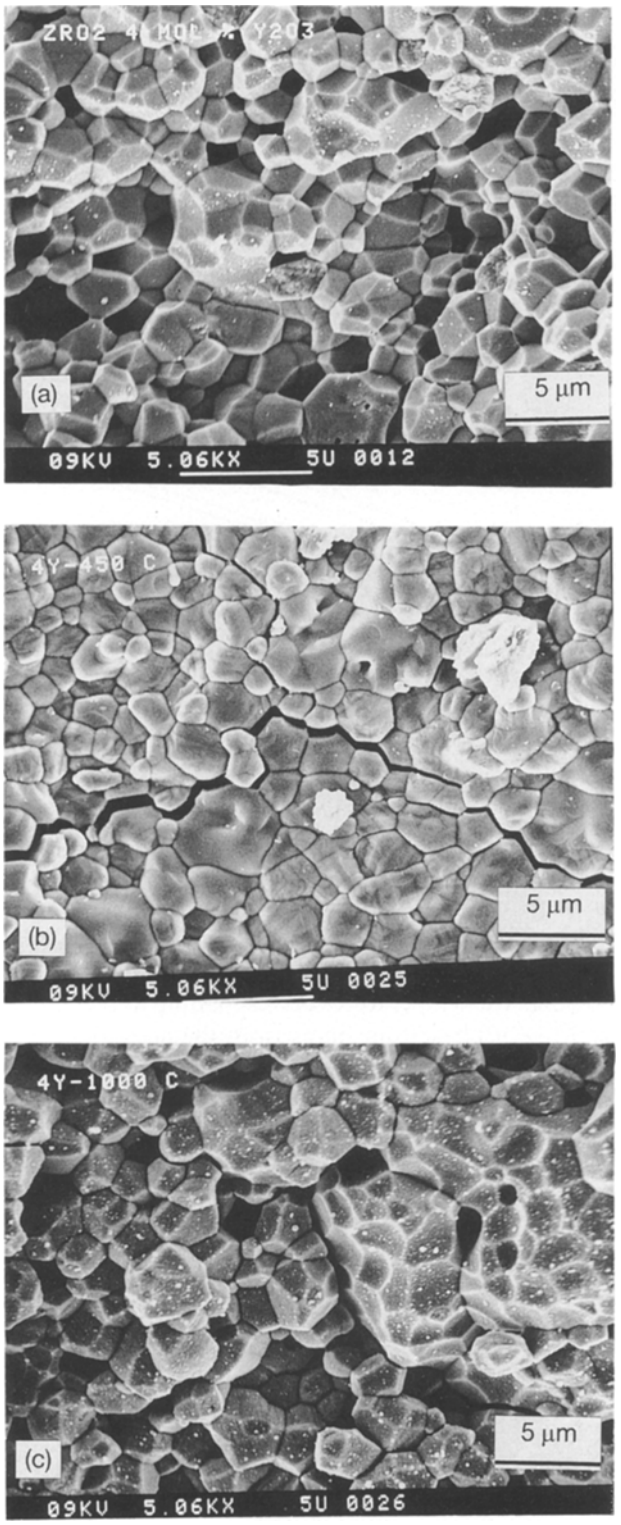

Figure 9 Scanning electron micrographs of ZrO_2–4 mol% Y_2O_3 sample (a) as sintered and after dilatometric runs up to (b) 450 °C and (c) 1000 °C.

cycle compared to the transformation of the smaller amount of the remaining metastable tetragonal phase during the second cycle of heating.

Similar data on two cycles of heating the 4 mol% Y_2O_3 sample to 400 °C are shown in Fig. 5a and c together with the corresponding dilatometric data (Fig. 5b), which indicate that the temperature of maximum acoustic emission activity coincides with the temperature of the start of the sudden dimensional expansion. As in the case of the 3 mol% Y_2O_3 sample, there was also no significant acoustic emission activity during cooling of the 4 mol% Y_2O_3 sample (not shown). The acoustic emission results on heating a 4 mol% Y_2O_3 sample to 1000 °C for the first time show intense acoustic emission activity at about 250 °C (Fig. 8a) and no significant acoustic emission counts at 250 °C during the second heating (Fig. 8b) as well as during the cooling cycles (Fig. 8c and d). Thus the acoustic emission data from several experiments on 3 and 4 mol% Y_2O_3 samples are similar.

Scanning electron micrographs of the ZrO_2–4 mol% Y_2O_3 sample after dilatometric measurement up to 450 °C show extensive intergranular microcracking (Fig. 9b) which is absent in the same sample in the as-sintered condition (Fig. 9a). The sample after a dilatometric experiment up to 1000 °C shows much less microcracking (Fig. 9c) than after cooling from 450 °C, suggesting that considerable healing of the microcracks generated on heating to low temperatures ($\leqslant$ 450 °C) has taken place by heating to and cooling from 1000 °C. The volume expansion accompanying the t → m phase change during cooling possibly contributes to the crack healing process.

3.2. Phase relations in the low-Y_2O_3 portion of the ZrO_2–Y_2O_3 system

The phase diagram of the low-Y_2O_3 portion of the ZrO_2–Y_2O_3 system, due to Srivastava *et al.* [42], is shown in Fig. 1, which is in agreement with other published phase diagrams [41, 43–45] except for the fact that the metastable tetragonal phase observed in a limited range of compositions is not shown here. In the present study, ZrO_2 compositions with 1–12 mol% Y_2O_3 were studied via X-ray diffraction, dilatometry and acoustic emission on heating and cooling. The X-ray diffraction data, shown in Fig. 2, were used to estimate the relative amounts of the monoclinic, (metastable) tetragonal and cubic phases (Table II). The sample with 1 mol% Y_2O_3 shows essentially monoclinic ZrO_2 solid solution. The amount of the monoclinic phase decreases gradually with increasing Y_2O_3 content till only a small amount of it is present in the 6 mol% Y_2O_3, and it is completely absent in the 9 and 12 mol% Y_2O_3 samples. The cubic phase increases with Y_2O_3 content such that 9 and 12 mol% Y_2O_3 compositions show pure cubic phase. As discussed earlier, 2, 3 and 4 mol% Y_2O_3 samples show some amount of metastable tetragonal phase in the as-sintered condition. The average grain size (1.5–2.0 μm) of these samples is above the reported critical grain size for the tetragonal phase [4] and therefore partial conversion to monoclinic phase has taken place, resulting in a mixture of m, t and c phases (Table II).

The thermal expansion behaviour of 1 and 2 mol% Y_2O_3 samples is depicted in Fig. 10 and of 6, 9 and 12 mol% Y_2O_3 samples in Fig. 11. Similar data for 3 and 4 mol% Y_2O_3 are already given in Figs 3 and 4.

The sintered samples of all these compositions were examined by acoustic emission during heating and

TABLE II Properties of sintered ZrO_2–Y_2O_3 compositions

Y_2O_3 (mol %)	α of cubic phase (10^{-6} °C^{-1})	Density (g cm^{-3})	Grain size (μm)	Phase composition (%)			AE data (°C)	
				m	t	c	m → t	t → m
1		5.213	2.1	95	5	–	846	710
2		5.198	1.98	70	15	15	600	565
3	12.5	5.192	1.875	33	42	25	565	565
4	10.7	5.094	1.51	24	43	33	565	565
6	11.68	5.112		13	–	87	565	565
9	12.1	5.189		–	–	100		
12	11.98	5.012		–	–	100		

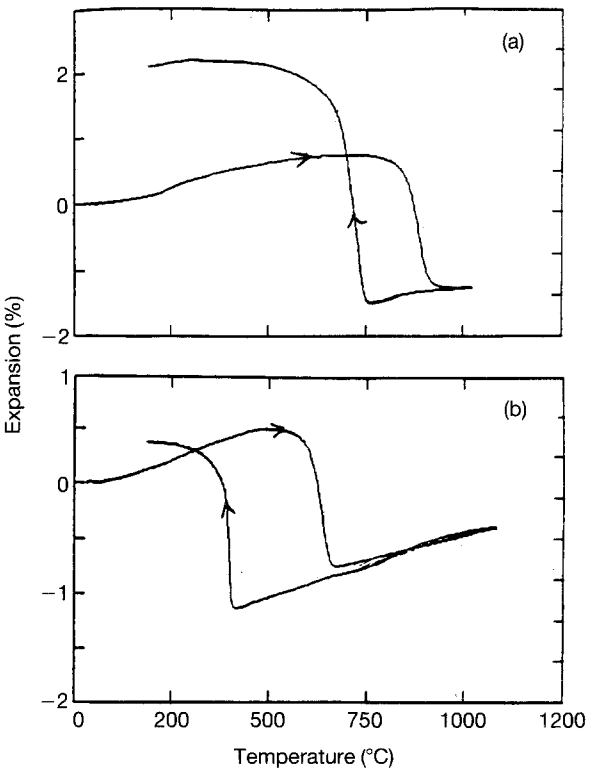

Figure 10 Thermal expansion behaviour of (a) 1 and (b) 2 mol% Y_2O_3 compositions.

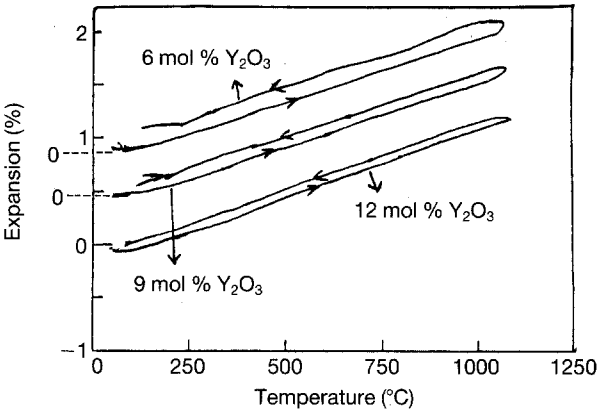

Figure 11 Thermal expansion behaviour of 6, 9, and 12 mol% Y_2O_3 compositions. The zero point of the expansion plot has been offset for the three samples.

cooling. The temperatures corresponding to the m → t and t → m phase transitions from the acoustic emission data for the compositions with 1–6 mol% Y_2O_3 are summarized in Table II. These transition temperatures are in reasonable agreement with Fig. 1. The acoustic emission data for 1 mol% Y_2O_3 shows intense acoustic emission activity at 835–840 °C on heating (Fig. 12a) and occurs at 708 °C and below on

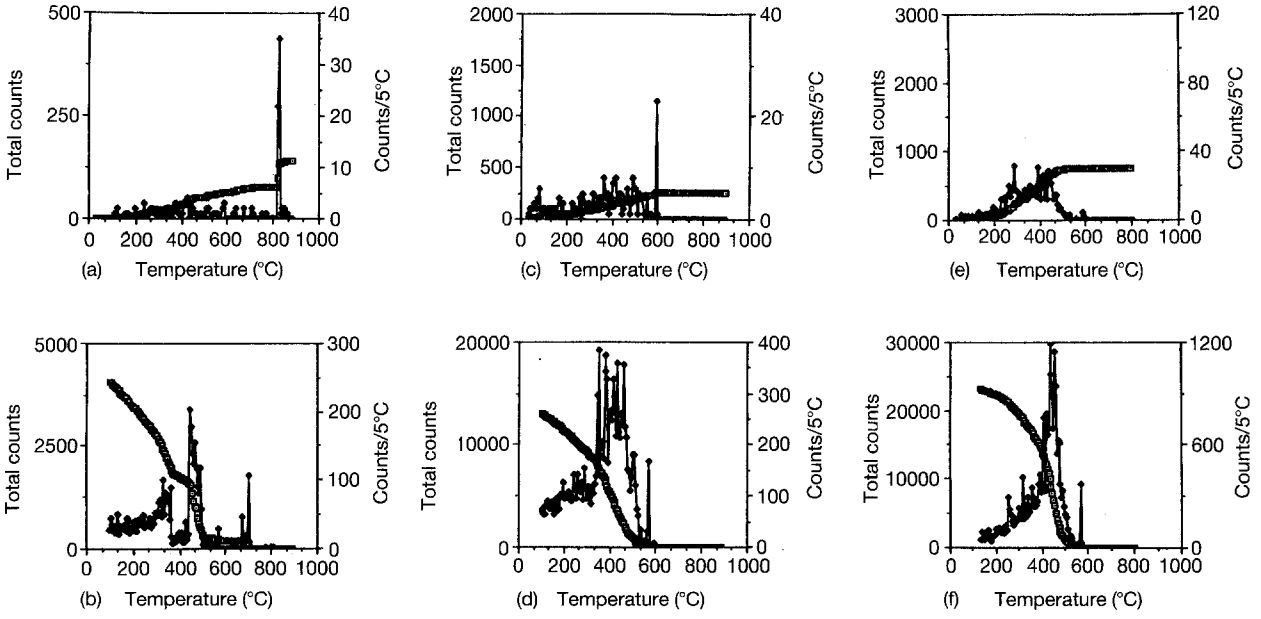

Figure 12 Acoustic emission data of 1, 2 and 6 mol% Y_2O_3 samples (a, c, e) during heating to 900 °C and (b, d, f) cooling, respectively: (□) total counts, (◆) counts per 5 °C.

cooling (Fig. 12b), which appears to correspond to m → t and t → m transitions, respectively (Table II). In the case of 2 (Fig. 12c and d), 3, 4 (Figs 3 and 7) and 6 mol% Y_2O_3 (Fig. 12e and f), intense acoustic emission activity starts at 570 ± 5 °C on heating and cooling (Table II). Interestingly, this temperature coincides with the eutectoid temperature reported by Srivastava *et al.* [42]. No significant acoustic emission activity was observed on heating and cooling of samples with 9 and 12 mol% Y_2O_3, and this is consistent with the fact that they are purely cubic phases undergoing no phase changes.

The acoustic emission data thus are in agreement with the phase relationships in this system established by quenching, X-ray diffraction and other conventional methods.

4. Conclusions

The acoustic emission technique is shown to be a sensitive tool to determine phase transitions and microcracking in ZrO_2–Y_2O_3 ceramics. Using this method, the microcracking resulting from the volume change at the metastable tetragonal transition at about 250 °C in ZrO_2 alloys with 3 and 4 mol% Y_2O_3 has been clearly established. The onset of acoustic emission activity at the m → t and t → m transitions and at the eutectoid transformation at about 565 °C confirms the established phase relations in the low-Y_2O_3 portion of the ZrO_2–Y_2O_3 system. The acoustic emission results are corroborated by dilatometry, X-ray diffraction and scanning electron microscopy.

Acknowledgement

The authors are grateful to the Ben Franklin Technology Center of Central and Northern Pennsylvania for financial support under Project No. 90C. 1016R-1.

References

1. R. C. GARVIE, R. H. J. HANNINK and R. T. PASCOE, *Nature* **258** (1975) 703.
2. T. K. GUPTA, J. H. BECHTOLD, R. C. KUZNICKI, L. H. CADOFF and B. R. ROSSING, *J. Mater. Sci.* **12** (1977) 2421.
3. T. K. GUPTA, F. F. LANGE and J. H. BECHTOLD, *ibid.* **13** (1978) 1464.
4. F. F. LANGE, *ibid.* **17** (1982) 240.
5. *Idem, ibid.* **17** (1982) 225.
6. D. C. PORTER and A. H. HEUER, *J. Amer. Ceram. Soc.* **62** (1979) 298.
7. R. H. J. HANNING, K. A. JOHNSON, R. T. PASCOE and R. C. GARVIE, *Adv. Ceram.* **3** (1981) 116.
8. R. H. J. HANNING, *J. Mater. Sci.* **18** (1983) 457.
9. K. KOBAYASHI, H. KUWAJIMA and T. MASAKI, *Solid State Ionics* **3/4** (1981) 489.
10. T. SATO and M. SHIMADA, *J. Amer. Ceram. Soc.* **67** (1984) C212.
11. M. MATSUI, T. SOMA and I. ODA, *Adv. Ceram.* **12** (1984) 371.
12. K. TSUKUMA, Y. KUBOTA and T. TSUKIDATE, *ibid.* **12** (1984) 382.
13. M. WATANABE, S. IIO and I. FUKUURA, *ibid.* **12** (1984) 391.
14. K. NAKAJIMA, K. KOBAYASHI and Y. MURATA, *ibid.* **12** (1984) 399.
15. H. S. LU and S. Y. CHEN, *J. Amer. Ceram. Soc.* **70** (1987) 537.
16. R. E. LEE and A. H. HEUER, *ibid.* **71** (1988) 694.
17. M. RUHLE and A. H. HEUER, *Adv. Ceram.* **12** (1984) 14.
18. M. L. McCARTNEY and M. RUHLE, *Acta Metall.* **37** (1989) 1859.
19. T. SATO, S. OHTAKI, T. ENDO and M. SHIMADA, *J. Amer. Ceram. Soc.* **68** (1985) C320.
20. T. SATO, S. OHTAKI and M. SHIMADA, *J. Mater. Sci.* **20** (1985) 1466.
21. T. SATO and M. SHIMADA, *J. Amer. Ceram. Soc.* **68** (1985) 356.
22. *Idem, J. Mater. Sci.* **20** (1985) 3988.
23. M. YOSHIMURA, T. NOMA, K. KAWABATA and S. SOMIYA, *J. Mater. Sci. Lett.* **6** (1987) 465.
24. F. F. LANGE, G. L. DUNLOP and B. I. DAVIS, *J. Amer. Ceram. Soc.* **69** (1986) 237.
25. H. TUSUBAKINO, R. NOZATO and M. HAMAMOTO, *ibid.* **74** (1991) 440.
26. M. T. HERNANDEZ, J. R. JURADO, P. DURAN and J. L. G. FIERRO, *ibid.* **74** (1991) 1254.
27. Y. MURASE and E. KATO, *ibid.* **66** (1983) 196.
28. A. J. A. WINNUBST and A. J. BURGGRAAF, *Adv. Ceram.* **24** (1988) 39.
29. S. ITO, M. WATANABE, K. KURODA, H. SAKA and T. IMURA, *ibid.* **24** (1988) 49.
30. T. SATO, S. OHTAKI, T. ENDO and M. SHIMADA, *ibid.* **24** (1988) 29.
31. H. SCHUBERT, N. CLAUSSEN and M. RUHLE, *Proc. Br. Ceram. Soc.* **34** (1984) 157.
32. P. J. WHALEN, F. REIDINGER and R. E. ANTRIM, *J. Amer. Ceram. Soc.* **72** (1989) 319.
33. T. TORAYA, M. YOSHIMURA and S. SOMIYA, *ibid.* **67** (1984) C119.
34. R. C. GARVIE and P. S. NICHOLSON, *ibid.* **55** (1972) 303.
35. V. SRIKANTH and E. C. SUBBARAO, *Acta Metal.* **40** (1992) 109.
36. E. C. SUBBARAO and V. SRIKANTH, *Physica C* **171** (1990) 449.
37. V. SRIKANTH, E. C. SUBBARAO, D. K. AGRAWAL, C-Y HUANG, R. ROY and G. V. RAO, *J. Amer. Ceram. Soc.* **74** (1991) 365.
38. R. E. WRIGHT, *ibid.* **55** (1972) 54.
39. Y. OHYA, Z. NAKAGAWA and K. HAMANO, *ibid.* **70** (1987) C184.
40. D. R. CLARKE and A. ARORA, *Adv. Ceram.* **12** (1984) 54.
41. M. YOSHIMURA, *Ceram. Bull.* **67** (1988) 1950.
42. K. K. SRIVASTAVA, R. N. PATIL, C. B. CHOUDHARY, K. V. G. K. GOKHALE and E. C. SUBBARAO, *Trans. J. Bri. Ceram. Soc.* **73** (1974) 85.
43. H. G. SCOTT, *J. Mater. Sci.* **10** (1975) 152.
44. C. PASCUAL and P. DURAN, *J. Amer. Ceram. Soc.* **66** (1983) 23.
45. R. RUH, K. S. MAZDIYASNI, P. G. VALENTINE and H. O. RIELSTEIN, *ibid.* **67** (1984) C190.

Received 28 October 1991
and accepted 24 March 1992